RESEARCH PAPER

PCCP
www.rsc.org/pccp

Photoelectron–photofragment coincidence study of OHF^-: transition state dynamics of the reaction OH + F → O + HF

Hans-Jürgen Deyerl[a] **and Robert E. Continetti***[b]

[a] *Institut für Physik, TU Chemnitz, D-09107 Chemnitz, Germany. E-mail: hans-juergen.deyerl@physik.tu-chemnitz.de; Fax: +49 (0) 371 531 3103; Tel: +49 (0) 371 531 3554*

[b] *Department of Chemistry and Biochemistry, University of California, San Diego, 9500 Gilman Drive, La Jolla, CA 92093-0340, USA. E-mail: rcontinetti@ucsd.edu; Fax: +1 858 534 7244; Tel: +1 858 534 5559*

Received 21st September 2004, Accepted 26th November 2004
First published as an Advance Article on the web 6th January 2005

A photoelectron–photofragment coincidence (PPC) study of the dissociative photodetachment of OHF^- at a photon energy of 4.80 eV is presented. The correlated electron kinetic energy (eKE) and translational energy release (E_T) into the O + HF + e^- products yield information on the potential energy surface close to the transition state of the neutral reaction OH + F → O + HF. The correlation spectrum shows two different features in the energetically allowed O + HF product channel: (a) diagonal ridges, resulting from direct dissociative photodetachment (DPD) and (b) areas with higher E_T in the neutral fragments from nonadiabatic dissociation. The total translational energy spectrum (E_{TOT} = eKE + E_T) reveals a vibrationally resolved product state distribution. These results are discussed in the context of recent theoretical studies of the dissociative photodetachment of OHF^-.

1. Introduction

The reactions of the hydroxyl radical, OH, play an important role in reactive environments including combustion processes and atmospheric chemistry. In particular the reactions with halogen atoms (X) are important in the catalytic ozone destruction cycle, leading to $O(^3P)$ + HX, since the hydrogen halides constitute the dominant temporary sink of atomic halogens.[1] Quantum calculations of the reaction dynamics of these systems require accurate potential energy surfaces, in particular close to the transition state of the reaction.[2,3] Recently, the potential energy surface of the benchmark system: $OH(^2\Pi)$ + $F(^2P)$ ↔ $O(^3P)$ + $HF(^1\Sigma^+)$ have been calculated using *ab initio* theory in two[4,5] and three dimensions.[6–8] In this report, photoelectron–photofragment coincidence studies of the dissociative photodetachment (DPD) of the OHF^- negative ion are used to probe this important region of the neutral potential energy surface.

DPD experiments carried out in our group on several OH radical reactions show that photoelectron–photofragment coincidence (PPC) spectroscopy provides unique information, in particular, the correlation between the kinetic energies of the photoelectron and the neutral fragments, on the dynamics of the reaction in the proximity of the transition state.[9–11] Accurate quantum dynamics calculations of the correlated photoelectron intensity and photofragment product energies have been carried out on the OH–H_2 system, revealing a detailed picture of the reaction dynamics.[12] To date, however, there have been no PPC measurements on that system, and similarly, no theoretical predictions for a system studied by the coincidence technique. Given the recent renewed theoretical interest in the OHF system,[7,13] experimental measurements on this system are timely and may provide the first opportunity for a detailed comparison of theory and experiment for the PPC measurements.

A number of previous experimental studies have been reported that probe the potential energy surface of the OH + F → O + HF reaction. Kinetics measurements by Walther and Wagner found a rate coefficient for the reaction of F + OH of 2.5×10^{13} cm^3 mol^{-1} s^{-1} at 300 K.[14] In an arrested relaxation IR-chemiluminescence study, Sloan *et al.*[15] obtained information on the product state distribution for the OH + F reaction. They observed product vibrational levels up to HF($v = 3$) in a study of the F + H_2O reaction. This was explained by secondary reactions of F with the nascent OH product of the F + H_2O reaction. The rotational and vibrational product state distribution from the secondary reaction appeared to be statistical. On the basis of *ab initio* calculations the authors concluded that the secondary reaction proceeds *via* an HOF complex on the singlet surface, since the barrier heights on the triplet surfaces were calculated to be too high to provide a reaction path.

Photodetachment of the hydrogen bonded anion OHF^- provides a route to exploration of the transition state region for the corresponding neutral bimolecular reaction OH + F → O + HF.[16] In photodetachment transition state spectroscopy experiments,[17–19] Franck–Condon analysis of the photodetachment spectrum in one and two dimensions has been used to test the potential energy surfaces for the anion complex and the neutral reaction. However, the photoelectron spectra measured for the OHF^- system measured by Bradforth *et al.*[16] were not fully explained prior to the recent work of González-Sánchez, *et al.*,[7,13] Bradforth *et al.* assigned the features in the photoelectron spectrum to the ν_3 hydrogen stretching mode correlating with states in the reactant and product channels based on 2D wavepacket simulations on approximate *ab initio* potential energy surfaces.[16] Dixon and Tachikawa[4] carried out a time-dependent wavepacket study of the dynamics of this system using 2D *ab initio* potential energy functions for collinear OHF^- and OHF. The simulated photoelectron spectra confirmed that Franck–Condon excitation of OHF^-

DOI: 10.1039/b414604b

prepares OHF in the transition state region for the bimolecular reaction OH + F ↔ O + HF on the lowest triplet ($^3\Pi$) surface.[4] The calculated product branching ratios indicated that each peak in the experimental photoelectron spectrum correlated with adiabatic dissociation to a single vibrational state of the OH(v) + F or O + HF(v) product. The highest electron energy peak observed by Bradforth *et al.* was not reproduced in these simulations.

González-Sánchez *et al.* have recently published two wave-packet dynamics studies of the OHF^- photodetachment spectrum.[7,13] In the most recent work in ref. 13, they have included for the first time the effects of multiple electronic states and the presence of Σ-Π conical intersections. In these recent simulations excellent agreement with the photoelectron spectra measured by Bradforth *et al.* in ref. 16 has finally been obtained, including the observation of a peak correlated with O + HF ($v = 0$) products. The calculated spectrum at larger photoelectron kinetic energies yielding products below the OH + F product channel showed a sequence of bands associated with vibrationally excited HF. Each band is formed by a continuous spectrum with overlapping resonances that are increasingly important for higher-lying product states. At lower energies, these resonances are primarily associated with the presence of wells in the O + HF product channel on the ground $^3A''$ surface.[7,13] At higher energies, the resonances change in character to heavy–light–heavy resonances and dominate the spectrum, in particular near the opening of the O + HF($v = 3,4$) product channels.[7,13] Even well below the OH + F product channel, however, at the threshold for O + HF($v = 2$) products, significant resonant features were predicted. While at higher levels of excitation, both singlet and triplet states were found to contribute to the observed dynamics, at low energies in a linear configuration only the $^3\Sigma^-$ and $^3\Pi$ states play an important role, and exhibit two conical intersections that can play a role in nonadiabatic dynamics.

The next step for comparison between theory and experiment in this system is to compare asymptotic product state distributions produced by dissociative photodetachment with theoretical predictions. This information, at a level of vibrational state resolution, is currently only obtainable from PPC experiments that measure the photoelectron kinetic energy and the photofragment translational energy from a given dissociation event *in coincidence*. Whereas photoelectron spectra alone can provide dynamic information through line broadening, the coincidence measurement of both photoelectron and photofragment energies directly determines the product channels accessed at a specific electron kinetic energy through energy conservation. In this paper, the first PPC experiments on the OHF^- system are reported.

Fig. 1 shows a schematic energetics diagram for the OHF^-/$O(^3P)$ + HF + e^- system. The potential surface of the OHF^- anion has been previously studied by means of *ab initio* theory.[4,5,7,16] The minimum geometry has a collinear configuration in which the shared proton is closer to the oxygen atom. The dissociation energies have been calculated to be $D_0(OHF^- \rightarrow OH + F^-) = 1.47$ eV and $D_0(OHF^- \rightarrow O^- + HF) = 2.05$ eV, respectively.[16] As discussed below, in this work we have determined the dissociation energy to be $D_0(OHF^- \rightarrow O^- + HF) = 1.90 \pm 0.1$ eV, in good agreement with the dissociation energy of the similar FHF^- anion: $D_0(FHF^- \rightarrow F^- + HF) = 1.93$ eV.[20] From the recommended thermochemical data in the NIST Webbook,[21] and the corrected value for the heat of formation for OH,[22] an exoergicity $\Delta E^0_0(O^- + HF \rightarrow F^- + OH) = 0.50$ eV is deduced. Using these data, a value of $D_0(OHF^- \rightarrow OH + F^-) = 1.40 \pm 0.1$ eV is found, in good agreement with the *ab initio* calculations described above. On the neutral surface, the reaction of OH with F is exothermic by ΔE^0_0 (OH + F → O + HF) = 1.45 eV.[21,22]

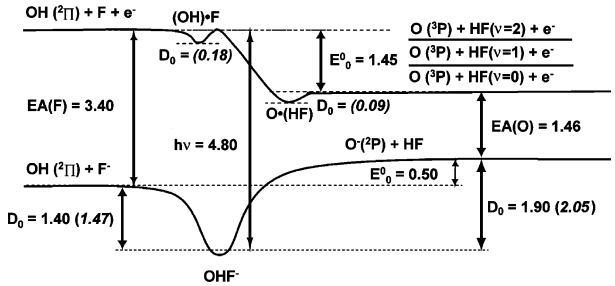

Fig. 1 Schematic energetics diagram for the OHF^-/F + OH + e^- system, all values are given in eV. The potential energy is shown as a function of a generic reaction coordinate. The electron affinities of fluorine and oxygen are EA(F) = 3.40 eV and EA(O) = 1.46 eV.[20] The values in parentheses are theoretically determined values. For details, see text.

The lowest triplet state potential energy surface of the neutral reaction has been calculated using *ab initio* methods in both two- ($^3\Pi$)[4,5,15,16] and very recently in three- dimensions ($^3A''$).[6–8] The 3D calculations at the multireference configuration-interaction level of theory show two hydrogen-bonded minima (OH)•F and O•(HF) close to the transition state of the reaction.[6,8] The dissociation energies of these minima have been calculated to be $D_0((OH)^\bullet F \rightarrow OH + F) = 0.18$ eV and $D_0(O^\bullet(HF) \rightarrow O + HF) = 0.09$ eV, respectively.[8] Moreover, the authors conclude that the reaction OH + F → O + HF has no barrier on the lowest triplet surface ($^3A''$) in a bent configuration.[6,8] In addition, relevant to the O + HF product channel, González-Sánchez *et al.* have now carried out calculations of the $^3\Sigma^-$ electronic state, which has two conical intersections with the previously studied $^3\Pi$ state along the reaction coordinate and also leads to ground state O + HF products.[13]

In the following sections we report a PPC study of the DPD of the OHF^- negative ion. In the present experiments, the laser energy of 4.80 eV only allows access to the $O(^3P)$ + $HF(^1\Sigma^+)$ product channel, with vibrational excitation in the HF product up to $v = 2$, as shown in Fig. 1. The signature of the correlation bands indicates direct adiabatic separation of the products along the reaction coordinate as well as evidence for nonadiabatic fragmentation into O + HF($v = 1$) products, possibly mediated by the conical intersections found by González-Sánchez *et al.*[13] From the total kinetic energy spectrum, the dissociation energy $D_0(OHF^- \rightarrow HF + O^-) = 1.90 \pm 0.1$ eV and the vibrationally resolved product state distribution for the O + HF product channel of the reaction is deduced.

2. Experimental

The fast beam photoelectron–photofragment coincidence spectrometer used in this study has been previously described in detail.[23] In the following paragraphs the experimental technique will be briefly reviewed. In these experiments, a fast beam of mass selected anions (OHF^-) was intersected with a pulsed laser beam, and the kinetic energies of the photodetached electrons and the neutral fragments were measured in coincidence using time- and position-sensitive detection techniques.

OHF^- was generated by crossing a supersonic expansion of HF (30% in H_2O) vapor seeded in N_2O with a 1 keV electron beam. The OHF^- formation mechanism is most likely *via* dissociative attachment of N_2O by slow secondary electrons $N_2O + e^- \rightarrow O^- + N_2$, followed by the clustering process $O^- + HF + M \rightarrow OHF^- + M$. The nascent ions were cooled in the supersonic expansion to a typical vibrational temperature of $T_{vib} \approx 450$ K [24] and a rotational temperature of $T_{rot} \approx 35$ K.[25] After passing through a skimmer into a differentially pumped chamber, the anions were accelerated to a beam energy of 5 keV. The continuous ion beam was chopped and referenced to ground potential and the anions mass-selected by time of flight (TOF).

Ions at $m/z = 36$ (OHF^-) were intersected at a right angle in the focus (diameter = 0.5 mm, pulse fluence = 5–10 mJ cm^{-2})

of a frequency tripled pulsed regeneratively amplified Ti:sapphire laser (258 nm, 1.2 ps FWHM, Clark-MXR CPA 2000). The *E*-vector of the linearly polarized light was aligned along the direction of the ion beam. Photodetached electrons were detected by one of two time- and position-sensitive wedge-and-strip-anode electron detectors, placed opposite to each other and perpendicular to the ion beam and the laser beam, respectively. Measurement of the electron recoil angle allowed correction of the Doppler broadening due the fast ion beam and the actual flight path, allowing determination of the electron kinetic energy (eKE) in the center of mass (CM) frame. The photoelectron spectrometer has an effective angular acceptance of $\approx$20% of 4 πsr and a resolution in eKE of $\approx$5% ΔeKE/eKE at 1.3 eV.[23]

Residual ions remaining in the beam after the interaction with the laser beam were electrostatically deflected out of the beam path to an ion detector providing the TOF spectrum of the negative ion beam. Neutral fragments of dissociative photodetachment (DPD) continued along the apparatus flight path and were detected with a photofragment translational spectrometer. The fragments recoiled out of the beam over a 104 cm flight path and impinged on a time- and position-sensitive crossed-delay-line multiparticle detector, allowing determination of the recoil velocities of the two particles in coincidence. This information yielded the photofragment mass ratio and the CM translational energy (E_T). This detector has a translational energy resolution of $\approx$10% $\Delta E_T/E_T$ at 1.3 eV.[26]

Since the electron and the photofragments are measured in coincidence, the correlated kinetic energy of the products (O + HF + e^-) are recorded in one experiment. All recorded events that produce one electron and two momentum-matched photofragments are analyzed as correlated information for DPD, yielding the $N(E_T$,eKE) correlation spectrum.[27] Statistics based on spectrometer efficiency and count rate of the experiment ensure that the photoelectron and photofragments from each event are correlated, with a typical false coincidence rate of $\approx$5%.[27]

3. Results

The photoelectron photofragment correlation (PPC) spectrum ($N(E_T$,eKE)) at 258 nm (4.80 eV) for OHF^- is shown in Fig. 2 as a 2D histogram of the correlation between E_T along the *x*-axis and eKE along the *y*-axis. The photoelectron spectrum, shown as the projection along the *y*-axis, is consistent with that reported by Bradforth *et al.*,[16] but is shifted down by 1.02 eV due to the lower photon energy. The photoelectron spectrum shows broad irregularly spaced features at eKE = 1.25, 0.80, 0.30 and 0.15 eV. The peak at 0.15 eV has a contribution from laser-produced background. For further discussion we use the labels (A–C) for the features in the eKE spectrum introduced by Bradforth *et al.*[16] The photofragment translational energy release, $N(E_T)$, is shown as the projection along the *x*-axis and exhibits a broad peak centered at E_T = 0.12 eV and a small shoulder at 0.375 eV. In the following paragraphs, the energetic implications of the coincidence spectrum are discussed, along with alternative ways of viewing the coincidence data. The eKE-selected photofragment $N(E_T)$ spectra and the total translational energy release spectra, $N(E_{TOT})$, presented can only be determined from the coincidence spectrum, and reveal vibrationally adiabatic and nonadiabatic contributions to the reaction dynamics.

The correlation of the bands in eKE and E_T reveals several features. The diagonal line in Fig. 2 marked as KE_{MAX} is drawn at the 5% level of the lowest contour, consistent with the level of false coincidences. This procedure was demonstrated to result in reliable dissociation energies for $O^-(H_2O)_2$ and $OH^-(H_2O)_2$.[28] KE_{MAX} represents the maximum available energy (eKE + E_T) for the three (O + HF (υ = 0) + e^-)

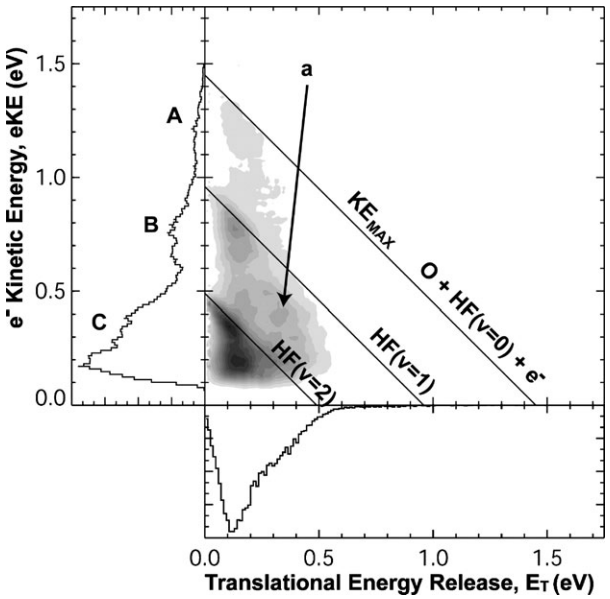

Fig. 2 Photoelectron–photofragment correlation (PPC) spectrum, $N(E_T$,eKE), for the reaction $OHF^- + h\nu \rightarrow O(^3P) + HF + e^-$ at 258 nm. The diagonal lines represent the onset of the energetically allowed $O(^3P)$ + HF(υ = 0,1,2) product states. The darker grey-scale features correspond to higher intensity with a linear scale. The features and energetic limits shown are discussed in the text. The arrow marked 'a' denotes the region where significant non-adiabatic dissociation leads to the production of O + HF(υ = 1) products above the threshold for O + HF(υ = 2).

products in the DPD, *e.g.* the product asymptote at a given laser energy $h\nu$ (258 nm)

$$KE_{MAX} = h\nu - D_0(OHF^- \rightarrow O^- + HF(\upsilon = 0)) - EA(O)$$
$$= 1.45 \pm 0.1 \text{ eV} \quad (1)$$

From this energy and the well known electron affinity of the oxygen atom (EA(O) = 1.46 eV) we can determine the dissociation energy $D_0(OHF^- \rightarrow O^- + HF) = 1.90 \pm 0.1$ eV in reasonable agreement with previous *ab initio* calculations of $D_0(OHF^- \rightarrow O^- + HF) = 2.05$ eV.[5,16] Starting from KE_{MAX} at 1.45 eV, diagonal limits can be drawn for the two energetically higher lying asymptotes for O + HF (υ = 1) + e^- at 0.96 eV and O + HF (υ = 2) + e^- at 0.49 eV, respectively. The dominant features observed in the $N(E_T$,eKE) spectra are three diagonal ridges, with high intensity along the diagonal energetic limits for the O + HF(υ = 0,1,2) dissociation asymptotes. The simplest explanation of these features is that they correspond to direct dissociative photodetachment (DPD) onto vibrationally adiabatic curves in the vicinity of the transition state for the neutral bimolecular reaction, correlating with the different vibrational states of the HF (υ = 0,1,2) product as predicted by theory.[4,7,16] In addition, for 0.15 < eKE < 0.55 eV, there is a significant feature appearing in Fig. 2 at larger translational energy release (E_T) compared to the main diagonal ridges, between the diagonal O + HF(υ = 1) and O + HF(υ = 2) energetic limits. This is evidence for a vibrationally nonadiabatic process playing a role in this system.

The results in the correlation spectrum can also be displayed by plotting the $N(E_T)$ distribution of the kinetic energy release between the neutral fragments integrated over different ranges of the photoelectron kinetic energy, eKE. These spectra are shown in Fig. 3 for four regions of the eKE distribution, and can be compared with the integrated $N(E_T)$ spectrum shown in the projection along the *x*-axis of Fig. 2. The results are summarized in Table 1. Examination of the $N(E_T)$ distribution for each feature individually shows that in addition to the expected inverse relationship between eKE and E_T, the peaks, widths and shapes of the spectra depend on the accessed product state. The first $N(E_T)$ curve corresponds to region A

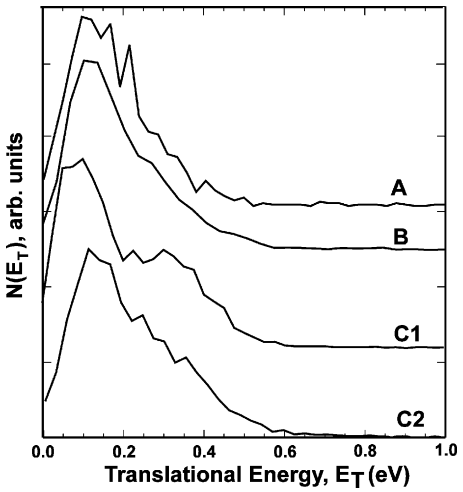

Fig. 3 The kinetic energy release ($N(E_T)$) distribution for specific ranges of the photoelectron kinetic energy, eKE. The peak positions are presented in Table 1. The eKE ranges for each curve are as follows: (A) 0.96–1.45 eV; (B) 0.49–0.95 eV; (C1) 0.30–0.49 eV and (C2) 0.0–0.29 eV.

in the eKE spectrum, integrated over the range 0.95 < eKE < 1.45 eV. This distribution peaks at 0.15 eV and extends to E_T = 0.55 eV, and represents the region where only O + HF($\upsilon = 0$) products are energetically available. The second $N(E_T)$ curve, B, representing the range 0.49 < eKE < 0.95 eV, contains both O + HF($\upsilon = 0,1$) products. This distribution peaks at 0.12 eV and extends beyond 0.6 eV. The third $N(E_T)$ curve, C1, in the range eKE = 0.30–0.49 eV reveals a bimodal distribution, with a peak at 0.10 eV and a secondary maximum at $E_T = 0.30$ eV. This region contains both the vibrationally adiabatic O + HF($\upsilon = 2$) product channel at low E_T, and the O + HF($\upsilon = 1$) channel at larger E_T. Finally, curve C2 represents the lowest eKE range, from 0.0–0.29 eV. Here the peak in the distribution remains low (0.11 eV), however the entire distribution is more skewed to the higher E_T products that are energetically available at such low eKEs. Significant signal in this eKE range is observed up to $E_T = 0.80$ eV, and originates from O + HF ($\upsilon = 1, 2$) products.

Another informative way to view the correlated $N(E_T$,eKE) distribution is by direct examination of the total translational energy release among the products. This spectrum is generated by summing the translational energy release and the photoelectron kinetic energy for each event: $E_{TOT} = E_T$ + eKE. The $N(E_{TOT})$ spectrum for $OHF^- + h\nu \rightarrow O + HF + e^-$ is shown in Fig. 4. Energy conservation dictates that this spectrum directly represents the O + HF product state distribution. The vertical limits marked on this spectrum at 1.45, 0.96 and 0.49 eV are identical to the diagonal limits for O + HF($\upsilon = 0, 1, 2$) + e^- originally shown in Fig. 2. Since there is diagonal structure in the $N(E_T$,eKE) correlation spectrum, the $N(E_{TOT})$ spectrum must show more resolved structure than the N(eKE) spectrum alone, as observed by comparison to the projection of the correlation spectrum on the eKE axis in Fig. 2. The $N(E_{TOT})$ distribution reveals a step-like function, corresponding to the O + HF($\upsilon = 0, 1, 2$) product state distribution.

Table 1 Peak positions in the eKE-selected $N(E_T)$ spectra

eKE energy range/eV	Peak $N(E_T)$ position/eV	Width/comments
0.00–0.29	0.11	Curve C2
0.30–0.49	0.10, 0.30	Curve C1
0.49–0.95	0.12	Curve B
0.96–1.45	0.10	Curve A
0.00–1.45	0.11	Entire eKE range, see Fig. 2

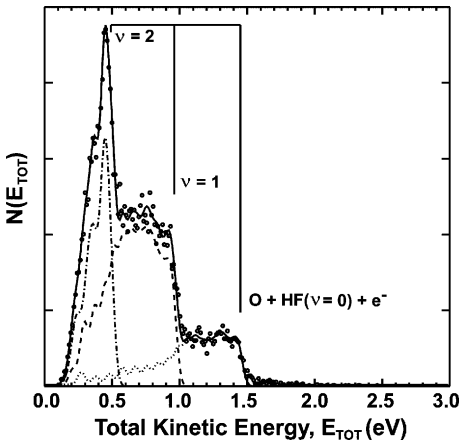

Fig. 4 Total translational energy release $N(E_{TOT})$ spectrum, showing the product state distribution for the DPD of OHF^- at 258 nm. The vertical lines are the energetic limits for the energetically allowed O + HF($\upsilon = 0, 1, 2$) product states. Approximate fits for the product O + HF(υ,J) states are shown as discussed in the text.

Evidently for $\upsilon = 0$ and 1 there is a large distribution of HF(υ,J) rotational states, causing these to overlap with the higher vibrational levels. The narrow feature at $E_{TOT} = 0.43$ eV dominates the spectrum, and arises from the intense diagonal feature observed in the $N(E_T$,eKE) spectrum at low E_T right below the O + HF($\upsilon = 2$) threshold. Some of the signal below this feature corresponds to laser-correlated background which is not easily removed from the correlation spectrum, however, given that the N(eKE) distribution observed in Fig. 2 is consistent with that reported by Bradforth *et al.* in ref. 16, this is estimated to not be more than 10–15% of the area under this peak.

Given that the vibrational features strongly overlap, it is not possible to extract an unambiguous product state distribution from the spectrum. Nonetheless, it is of interest to fit the spectrum with a series of Gaussian functions ($\sigma = 0.03$ eV) centered at each product O + HF(υ,J) state to gain insights into an approximate distribution and product branching ratio. The fit shown in Fig. 4 assumes that the rotational distributions for HF($\upsilon = 0$) and HF($\upsilon = 1$) are identical, and yields an approximate product vibrational state distribution of HF ($\upsilon = 0$) : HF($\upsilon = 1$) : HF($\upsilon = 2$) of 0.21 : 0.52 : 0.28. The rotational distributions for HF($\upsilon = 0$) and HF($\upsilon = 1$) are broad and peak at $J = 12$ in both cases. The HF($\upsilon = 2$) branching ratio is probably reduced by the eKE = 0.1 eV cut-off in the data obtained at this wavelength.

4. Discussion

The photoelectron photofragment coincidence spectra described in this paper provide detailed experimental insights into the half collision dynamics in the dissociative photodetachment (DPD) of OHF^- into the O + HF + e^- product channel. As shown by the *ab initio* calculations of Dixon and Tachikawa,[4] and González-Sánchez *et al.*[7] photodetachment of OHF^- indeed produces the nascent neutral OHF complex near the transition state for the OH + F → O + HF hydrogen exchange reaction, as first proposed by Bradforth *et al.*[16] At the photon energy used in this study, Fig. 1 shows that there is insufficient energy available to reach the OH + F product channel, so the dynamics observed in this experiment occur solely in the O + HF product channel. The calculations of González-Sánchez *et al.*[13] show that in this energy range both direct DPD and resonances mediated by wells on the neutral potential energy surface play a role in the dynamics. The photoelectron kinetic energy resolution in the present experiments is insufficient to resolve the predicted resonance features, however, these coincidence experiments provide clear evidence

for nonadiabatic processes related to the predicted resonances and the interaction of multiple potential energy surfaces.

The previously measured photoelectron spectrum N(eKE)[16] and the photofragment translational energy release spectrum $N(E_T)$ presented here are both of considerable value in understanding the dynamics of this system. However, the photoelectron–photofragment correlation spectrum $N(E_T$,eKE) shown in Fig. 2 shows how energy conservation and the reaction dynamics of the system connect the transient complexes produced by photodetachment near the transition state with the asymptotic product channels. The photoelectron spectrum N(eKE) is determined by the Franck–Condon overlap between the bound anion wavefunction and the scattering wavefunction on the neutral surface. The $N(E_T$,eKE) correlation spectrum provides the additional information tying the Franck–Condon region on the neutral surface reached by photodetachment with the dissociation dynamics and final product state distribution.

The dynamics leading to the O + HF products in the DPD of OHF^- at 258 nm are more complex than those observed in the OH + OH and OH + H_2O systems previously studied in our laboratory.[9,10] In these earlier cases, direct dissociative photodetachment onto repulsive vibrationally adiabatic potential energy surfaces near the transition state for the neutral bimolecular reaction could explain the energy partitioning observed in the $N(E_T$,eKE) correlation spectra—the excitation induced by photodetachment is carried over into the final state. In the O + HF case, once again significant diagonal features are observed in the correlation spectrum at the thresholds for the HF product vibrational states. However, particularly at eKEs at and below the energetic threshold for O + HF(v = 2) products, a significant signal is seen in Fig. 2 at higher E_T, corresponding to the production of O + HF(v = 1) products. Furthermore, these products are produced with much higher rotational excitation, as the signal is significantly displaced from the O + HF(v = 1) energetic limit in the correlation spectrum in Fig. 2. This is evidence for a significant breakdown of vibrational adiabaticity in the O + HF product channel. The bimodal shape of curve C1 in the $N(E_T)$ spectra for the eKE range between 0.30 and 0.49 eV provides another graphic example of the magnitude of this effect.

The breakdown of vibrational adiabaticity, when compared to the OH + H_2O system may be a result of the considerably more complicated electronic structure in the OH + F → O + HF system. Hydrogen atom transfer in the OH + H_2O system involves only one open shell species in both reactants and products, and near threshold occurs solely on the lowest $^2A'$ potential energy surface. The $^2A''$ surface is 0.58 eV higher in energy and is thus not expected to play a significant effect near threshold.[29] The OH + OH → O + H_2O system, however, has a comparable level of electronic complexity, yet also is dominated by vibrationally adiabatic dissociative photodetachment. As Harding showed, the $^3A'$ and $^3A''$ states on the OH + OH potential energy surface lie within 0.1 eV of one another and thus might be expected to strongly interact.[30] Nonetheless, the OH + OH → O + H_2O system does not exhibit a breakdown in vibrational adiabaticity such as that observed in the present experiments for the O + HF → OH + F system. The most likely cause for the experimentally observed vibrational nonadiabaticity is found in the recent multi-surface 3D simulations of the DPD of OHF^- by González-Sánchez *et al.*[13] They found that in a collinear configuration $^3\Sigma^-$ and $^3\Pi$ states correlating with O + HF products have two conical intersections along the reaction coordinate, providing the opportunity for vibronic effects leading to a breakdown of vibrational adiabaticity.

The parent anion potential energy surface determines directly the region of the neutral surface probed in a DPD experiment, and Dixon and Tachikawa showed that parent anion vibrational excitation had a significant effect on the photoelectron spectra and branching ratios in the DPD of OHF^-.[4] They carried out wavepacket dynamics simulations of the spectrum in cases with excitation of the low-frequency O–F stretching vibration (ν_1, 433 cm^{-1})[16] and the much higher frequency O–H–F ν_3 mode (ν_3, 2015 cm^{-1}).[16] Bradforth *et al.* calculated the bending frequencies for linear OHF^- to be 1064 and 1225 cm^{-1} at the UMP2/6-31++G** level of theory.[16] As expected, distortion from the collinear geometry in the anion leads to $^2A'$ and $^2A''$ states which are included in the recent calculations of González-Sánchez *et al.*[13] Assuming a vibrational temperature of 450 K, excitation of the low-frequency O–F vibration may be on the order of 25%. However, this is likely an upper limit as these low frequency vibrations may cool more effectively in the supersonic jet expansion ion source. In any case, based on these considerations, inclusion of rotational, vibrational and electronic averaging may all play an important role in more accurate simulations of the photodetachment experiment.

As noted in the $N(E_{TOT})$ spectrum in Fig. 4, there is significant rotational excitation observed in the O + HF(v = 0, 1) levels. Dixon and Tachikawa noted that on the *ab initio* neutral surface used in their wavepacket calculations, the bending potential was quite flat and that any product rotation was expected to arise from bend excitation in the anion as opposed to a torque on the neutral surface.[4] However, in the recent study of reactive collisions of F + OH on the lowest $^3A''$ surface, Gomez-Carrasco *et al.* find an O–H–F angle of 109.2° for the transition state geometry,[8] indicating that the dynamics on the neutral surface may play an important role in the distribution of HF rotational states. The final rotational distribution is also likely to be very sensitive to the conical intersections predicted for this system, so theoretical predictions of the rotational state distribution for the open HF vibrational levels are of significant interest.

Finally, the assignment of peak A in the photoelectron spectrum to O + HF(v = 0) needs examination. As discussed in the introduction, the energetics found in this experiment for the dissociation energy $D_0(OHF^- \rightarrow O^- + HF) = 1.90 \pm 0.1$ eV are consistent with previous theoretical predictions and comparable with the dissociation energy of similar systems such as FHF^-. This indicates that the assignment of KE_{MAX} to the production of O + HF(v = 0) + e^- is very reasonable, and is supported by the observation that the product state distribution represented by the $N(E_{TOT})$ spectrum in Fig. 4 has new features precisely at the thresholds for HF(v = 1,2). In the 2D wavepacket calculations of Dixon and Tachikawa, however, the O + HF(v = 0) transition was assigned to peak B, concluding that peak A 'cannot correspond to the most probable transition to O + HF(v = 0)' because of the 0.6 eV repulsive energy predicted on the neutral surface at the anion geometry.[4] This question appears to have been resolved in the recent calculations of González-Sánchez *et al.*,[13] as they showed that peak A arises from the previously neglected $^3\Sigma^-$ surface. This surface exhibits a significant well along the reaction coordinate, consistent with the low E_T measured between the neutral products for this feature in the present coincidence experiments.

5. Conclusion

In summary, we report a study of the dissociative photodetachment (DPD) of the OHF^- anion at 258 nm using PPC spectroscopy. Photodetachment at this wavelength yields only O(^{3}P) + HF($^1\Sigma^+$, v = 0, 1 and 2) products. These measurements provide insights into the half collision dynamics of the neutral hydrogen abstraction reaction: OH($^2\Pi$) + F(^{2}P) → O(^{3}P) + HF($^1\Sigma^+$). The correlated spectra reveal a resolved sequence of bands associated with vibrational excitation of HF up to v = 2. The diagonal correlation bands observed at each product vibrational threshold are consistent with direct DPD on adiabatic potential surfaces connecting product O + HF(v) levels

with vibrationally excited species near the transition state for the bimolecular reaction. In addition, above the O + HF($v = 2$) threshold, a significant signal is observed consistent with a breakdown of the vibrational adiabaticity as observed by an increase in the translational energy release associated with decomposition to the O + HF($v = 1$) product channel. These vibrationally nonadiabatic products may be the result of the conical intersections predicted for the $^3\Sigma^-$ and $^3\Pi$ states that correlate with O + HF products. These new experimental results provide a new challenge to theory for this benchmark system. Future experimental efforts to study the DPD of OHF^- at higher photon energies should provide insights into the transition state dynamics leading to the higher energy OH + F product channel as well.

Acknowledgements

This work was supported by the Department of Energy (DOE) under Grant No. DE-FG03-98ER14879. H.J.D. gratefully acknowledges partial support from a Forschungsstipendium sponsored by the Deutsche Forschungsgemeinschaft (DE 732/1-1) and the DOE.

References

1 R. P. Wayne, *Chemistry of Atmospheres*, Oxford University Press, Oxford, 3rd edn., 2000.
2 D. C. Clary, *Science*, 1998, **279**, 1879.
3 D. H. Zhang, M. A. Collins and S. Y. Lee, *Science*, 2000, **290**, 961.
4 R. N. Dixon and H. Tachikawa, *Mol. Phys.*, 1999, **97**, 195.
5 N. Elghobashi and L. González, *Phys. Chem. Chem. Phys.*, 2004, **6**, 4071.
6 S. Gómez-Carrasco, L. González-Sánchez, A. Aguado, M. Paniagua, O. Roncero, M. L Hernández and J. M. Alvariño, *Chem. Phys. Lett.*, 2004, **383**, 25.
7 L. González-Sánchez, S. Gómez-Carrasco, A. Aguado, M. Paniagua, M. L. Hernández, J. M. Alvariño and O. Roncero, *J. Chem. Phys.*, 2004, **121**, 309.
8 S. Gómez-Carrasco, L. González-Sánchez, A. Aguado, O. Roncero, J. M. Alvariño, M. L. Hernández and M. Paniagua, *J. Chem. Phys.*, 2004, **121**, 4605.
9 H. J. Deyerl, A. K. Luong, T. G. Clements and R. E. Continetti, *Faraday Discuss.*, 2000, **115**, 147.
10 H. J. Deyerl, T. G. Clements, A. K. Luong and R. E. Continetti, *J. Chem. Phys.*, 2001, **115**, 6931.
11 T. G. Clements, R. E. Continetti and J. S. Francisco, *J. Chem. Phys.*, 2002, **117**, 6478.
12 D. H. Zhang, M. Yang, M. A. Collins and S. Y. Lee, *Proc. Natl. Acad. Sci. USA*, 2002, **99**, 11579.
13 L. González-Sánchez, S. Gomez-Carrasco, A. Aguado, M. Paniagua, M. Luz Hernandez, J. M. Alvarino and O. Roncero, *J. Chem. Phys.*, 2004, **121**, 9865.
14 C. D. Walther and H. G. Wagner, *Ber. Bunsen-Ges. Phys. Chem.*, 1983, **87**, 403.
15 J. J. Sloan, D. G. Watson, J. M. Williamson and J. S. Wright, *J. Chem. Phys.*, 1981, **75**, 1190.
16 S. E. Bradforth, D. W. Arnold, R. B. Metz, A. Weaver and D. M. Neumark, *J. Phys. Chem.*, 1991, **95**, 8066.
17 D. M. Neumark, *Annu. Rev. Phys. Chem.*, 1992, **43**, 153.
18 R. B. Metz, S. E. Bradforth and D. M. Neumark, *Adv. Chem. Phys.*, 1992, **81**, 1.
19 D. M. Neumark, *Acc. Chem. Res.*, 1993, **26**, 33.
20 P. G. Wenthold and R. R. Squires, *J. Phys. Chem.*, 1995, **99**, 2002.
21 NIST webbook, http://webbook.nist.gov/chemistry/ ~2003.
22 B. Ruscic, A. F. Wagner, L. B. Harding, R. L. Asher, D. Feller, D. A. Dixon, K. A. Peterson, Y. Song, X. Qian, C.-Y. Ng, J. Liu, W. Chen and D. W. Schwenke, *J. Phys. Chem. A*, 2002, **106**, 2727.
23 K. A. Hanold, A. K. Luong, T. G. Clements and R. E. Continetti, *Rev. Sci. Instrum.*, 1999, **70**, 2268.
24 M. C. Garner, K. A. Hanold, M. S. Resat and R. E. Continetti, *J. Phys. Chem. A*, 1997, **101**, 6577.
25 R. E. Continetti, D. R. Cyr, R. B. Metz and D. M. Neumark, *Chem. Phys. Lett.*, 1991, **182**, 406.
26 K. A. Hanold, A. K. Luong and R. E. Continetti, *J. Chem. Phys.*, 1998, **109**, 9215.
27 R. E. Continetti, *Int. Rev. Phys. Chem.*, 1998, **17**, 227.
28 T. G. Clements, A. K. Luong, H. J. Deyerl and R. E. Continetti, *J. Chem. Phys.*, 2001, **114**, 8436.
29 D. W. Arnold, C. Xu and D. M. Neumark, *J. Chem. Phys.*, 1995, **102**, 6088.
30 L. Harding, *J. Phys. Chem.*, 1991, **95**, 8653.

